

Atomic Coherent States and Sphere Maps

Robert Gilmore

Physics Department, Drexel University, Philadelphia, Pennsylvania 19104, USA

(Dated: November 11, 2011)

An atomic coherent state will evolve to an atomic coherent state under a classical driving field. Under a time-periodic driving field the phase space for the dynamics is $S^2 \times S^1$, so that chaotic motion is possible. We explore the types of motion that can occur for periodically driven atomic coherent states by investigating the properties of the first return map $S^2 \rightarrow S^2$. The sphere map that we introduce is a generalization of the Kolmogorov-Arnold circle map that is based on the Gauss sphere map. We find mixtures of mode-locking, quasiperiodicity, forward and reverse period-doubling cascades, and chaos.

I. INTRODUCTION

Atomic coherent states were initially introduced to describe the coherence properties of atoms in a laser cavity [1]. The hamiltonian used to describe the interacting atom-field system in the laser cavity is

$$H = \sum_{\mathbf{k}} \hbar\omega(\mathbf{k})(a_{\mathbf{k}}^\dagger a_{\mathbf{k}} + \frac{1}{2}) + \sum_j \frac{\epsilon}{2} \sigma_j^z + \sum_{\mathbf{k}} \sum_j \left(\lambda^*(\mathbf{k}) a_{\mathbf{k}}^\dagger \sigma_j^- e^{-i\mathbf{k}\cdot\mathbf{r}_j} + \lambda(\mathbf{k}) a_{\mathbf{k}} \sigma_j^+ e^{i\mathbf{k}\cdot\mathbf{r}_j} \right) \quad (1)$$

In this expression $a(\mathbf{k})^\dagger$ is the operator creating a photon of wave vector \mathbf{k} and energy $\hbar\omega(\mathbf{k})$, j indexes the individual atoms, for which only two levels are assumed to be important in laser processes, \mathbf{r}_j is the position of the j th atom and the energy difference between the two atomic levels in the absence of fields is ϵ . The Pauli spin operator σ_j^z describes the zero-field eigenstates of the j th atom, the interaction term $\lambda^*(\mathbf{k}) a_{\mathbf{k}}^\dagger \sigma_j^-$ describes the emission of a photon of wavenumber \mathbf{k} and the deexcitation of the j th atom, while $\lambda(\mathbf{k}) a_{\mathbf{k}} \sigma_j^+$ describes photon absorption and atomic excitation. It is usually assumed that there are N atoms and they are localized within a distance d over which the phases $e^{\pm i\mathbf{k}\cdot\mathbf{r}_j}$ do not vary significantly. The usual commutation relations apply: $[\sigma_j^z, \sigma_k^\pm] = \pm \sigma_j^\pm \delta_{jk}$, $[a_{\mathbf{k}}, a_{\mathbf{k}'}^\dagger] = \delta_{\mathbf{k},\mathbf{k}'}$. Polarization indices have been suppressed.

II. TWO SEMICLASSICAL THEOREMS

Equation (1) has two dual semiclassical limits. In one limit the atomic sources are assumed to be classical, so that the field is driven by a classical current. In this limit the sums over atoms can be replaced by classical currents $\sum_j \sigma_j^{\pm,z} \rightarrow j(t)^{\pm,z}$ and Eq. (1) can be replaced by the semiclassical limit

$$H_{\text{s.c. field}} = \sum_{\mathbf{k}} \hbar\omega(\mathbf{k})(a_{\mathbf{k}}^\dagger a_{\mathbf{k}} + \frac{1}{2}) + j_z(t) + \sum_{\mathbf{k}} \left(\lambda^*(\mathbf{k}) a_{\mathbf{k}}^\dagger j^-(t) + \lambda(\mathbf{k}) a_{\mathbf{k}} j^+(t) \right) \quad (2)$$

where $j^z(t)$ is real and $(j^-(t))^* = j^+(t)$. In this case the classical current produces a coherent field state [2, 3, 4, 5]. More specifically, if the field is initially in its ground state (no photons) then it will evolve into a field coherent state for all future times.

In the other limit the field is assumed to be classical, so that the field operators can be replaced by their expectation values $\sum_{\mathbf{k}} a(\mathbf{k})^\dagger \rightarrow f^*(t)$, and in this limit the semiclassical hamiltonian takes the form

$$H_{\text{s.c. atom}} = F(t) + \sum_j \frac{\epsilon}{2} \sigma_j^z + f^*(t) \sigma_j^- + f(t) \sigma_j^+ \quad (3)$$

In this case the classical field produces an atomic coherent state. This is emphasized by writing the sums over the individual atomic operators as an operator in the N -particle representation of the Lie group $SU(2)$ with angular

momentum quantum number $J = \frac{N}{2}$: $\sum_j \sigma_j^\pm \rightarrow J_\pm$, $\sum_j \sigma_j^z \rightarrow J_z$. The semiclassical hamiltonian assumes the simpler form (removing the floating energy $F(t)$):

$$H_{s.c. \text{ atom}} = \epsilon(t)J_z + f^*(t)J_- + f(t)J_+ \quad (4)$$

This linear time-dependent equation guarantees that if the atomic state of the system is initially a coherent state (all atoms in their ground states) it will evolve into a coherent state for all times in the future.

The two semiclassical theorems are dual and can be stated simply as follows [1]: Once a coherent state, always a coherent state under a semiclassical hamiltonian. In this sense (and many others) the atomic coherent states are dual to the older field coherent states [2, 3, 4].

III. PHASE SPACE

Atomic coherent states are obtained by applying an operation g from the group $SU(2)$ (we are working with 2-level atoms) to the ground state in a Hilbert space that carries an irreducible representation of this group. For an ensemble of N atoms the ground state in zero field is $|\frac{1}{2}, -\frac{1}{2}\rangle^{\otimes N} = |J, -J\rangle$, where $2J = N$. The coherent states $|J, \Omega\rangle$ are defined by

$$g|J, -J\rangle = \Omega h|J, -J\rangle = \Omega|J, -J\rangle e^{i(-J)\phi} = |J, \Omega\rangle e^{i(-J)\phi} \quad (5)$$

Elements $h \in U(1)$ modify the individual atom ground state $|\frac{1}{2}, -\frac{1}{2}\rangle$ by a phase factor $e^{i(-1/2)\phi}$. The remaining group operations, the coset representatives $\Omega = g/h \in SU(2)/U(1)$, exist in 1:1 correspondence with the $SU(2)$ coherent states in the irreducible representation with $J = N/2$. The quotient space $SU(2)/U(1)$ is equivalent to the two-sphere: $SU(2)/U(1) \simeq S^2$ [1].

The point on the sphere surface that represents the coherent state $|J, \Omega\rangle$ moves under the influence of the Schrödinger time-dependent equation of motion:

$$i\hbar \frac{d}{dt} |J, \Omega\rangle = H_{s.c. \text{ atom}} |J, \Omega\rangle \quad \Rightarrow \quad |J, \Omega\rangle \rightarrow |J, \Omega(t)\rangle \quad (6)$$

If the semiclassical hamiltonian is independent of time the phase space is the sphere S^2 and the dynamics is asymptotically tame: asymptotic trajectories are fixed points or limit cycles. The evolution of the coherent state is described by a rigid rotation of the sphere around an axis determined by the semiclassical hamiltonian, and the unitary transformation is $U(t) = \exp(-\frac{i}{\hbar} H_{s.c. \text{ atom}} t)$.

If the semiclassical hamiltonian is periodic the phase space is enlarged to $S^2 \times S^1$ [6, 7]. Dynamical possibilities are enriched in this larger phase space: chaotic and quasiperiodic motion are also possible. We define chaotic motion as bounded (necessarily so in this compact phase space), recurrent but not periodic, and sensitive to initial conditions.

IV. SPHERE MAPS

Rather than attempt to study the full dynamics in $S^2 \times S^1$, we approach this problem by studying the properties of the first return map. The Poincaré section is defined stroboscopically as the constant phase section of the periodic driving field. This section is the sphere S^2 : as a result the first return map is a sphere map $S^2 \rightarrow S^2$ [8].

In order to define a sphere map we use the circle map $S^1 \rightarrow S^1$ as a model. The circle map is [9, 10]

$$\theta_{n+1} = \omega_0 + \theta_n + k \sin(\theta_n) \quad (7)$$

In this map θ_n is a point on the circle, observed as the n th stroboscopic measurement. The parameter ω_0 describes a rigid rotation during each forcing period. The nonlinearity is described by the term $k \sin(\theta_n)$.

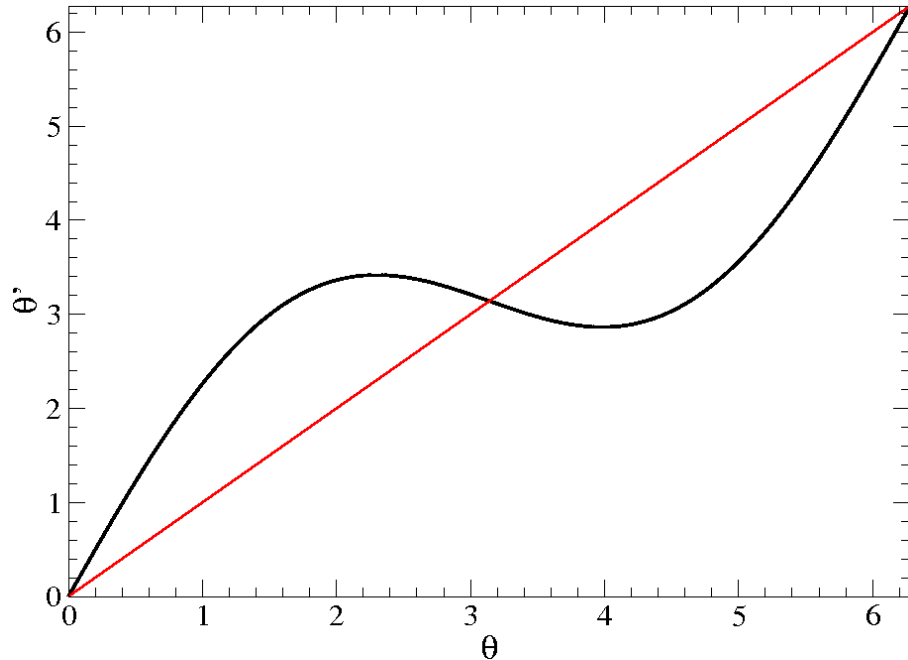


FIG. 1: First return map for the circle map $\theta' = \omega_0 + \theta + k \sin(\theta)$ for $k = 1.5$, with $\omega_0 = 0$. This map is singular (noninvertible) and exhibits a double-fold singularity $2A_2$.

The circle map can be regarded as the composition of two separate maps. One is a rigid rotation of the circle during each period: $\theta \rightarrow \theta + \omega_0$. The second map is the nonlinear map: $\theta \rightarrow \theta + k \sin(\theta)$, $0 \leq \theta \leq 2\pi$. The circle map has a two-fold rotation symmetry about $(\theta, \theta') = (\pi, \pi)$ (c.f., Fig. 1).

If we regard the circle map as the first map in a hierarchy of nonlinear maps of spheres to themselves, the next map in this class also involves two steps. The first is a rigid rotation of the sphere to itself. The second is a wrinkling of the surface of the sphere.

The rigid rotation of the sphere is carried out by an element in the Lie group $SO(3)$, which is the $2 \rightarrow 1$ image of $SU(2)$. The rigid rotation of the sphere surface to itself is represented by a 3×3 matrix [11, 12]

$$R(\mathbf{n}, \omega) = I_3 \cos \omega + \mathbf{L}(\mathbf{n}) \sin \omega + \mathbf{Q}(\mathbf{n})(1 - \cos \omega) \quad (8)$$

Here \mathbf{n} is a unit vector about which rotations through an angle ω are carried out and the parameter space is doubly connected since $R(\mathbf{n}, \pi) = R(-\mathbf{n}, -\pi)$ [11, 12]. The orbital angular momentum matrix has matrix elements $\mathbf{L}_{ij}(\mathbf{n}) = \epsilon_{ijk} n_k$ and the quadrupole matrix is defined by $\mathbf{Q}(\mathbf{n})_{ij} = n_i n_j$.

The nonlinear deformation of the sphere surface can conveniently be carried out using the Gauss map [13]. Gauss had the elegant idea of mapping a surface into the sphere surface by computing the unit normal to a surface at each point on a surface, and mapping that point on the surface to the sphere surface along the unit vector. In order to create a nonlinear deformation of the sphere surface, imagine pushing a finger into the sphere surface to deform it, and then applying the Gauss map to this deformed surface. We illustrate this idea by creating a circle map by deforming the circle. A simple deformation is obtained using the classical limaçon curve:

$$r(\theta) = 2 + a \cos(\theta) \quad (9)$$

For $a > 0$ the circle is pushed in toward the center around $\theta = \pi$. The deformation under the Gauss map is invertible for $0 \leq a < 1$ and noninvertible for $1 \leq a$. The curve is nonsingular for $|a| < 2$ and singular for $2 \leq |a|$. For $|a| < 2$ the index is 1 and for $|a| > 2$ the index is 2. The gauss map $\theta \rightarrow \theta'$ for the circle is shown in Fig. 2 for $a = 1.5$. This map is qualitatively similar to the Arnold circle map Eq. (7) shown in Fig. 1 for $k = 1.5$.

A deformation of the surface of a sphere is easily represented by the spherical limaçon

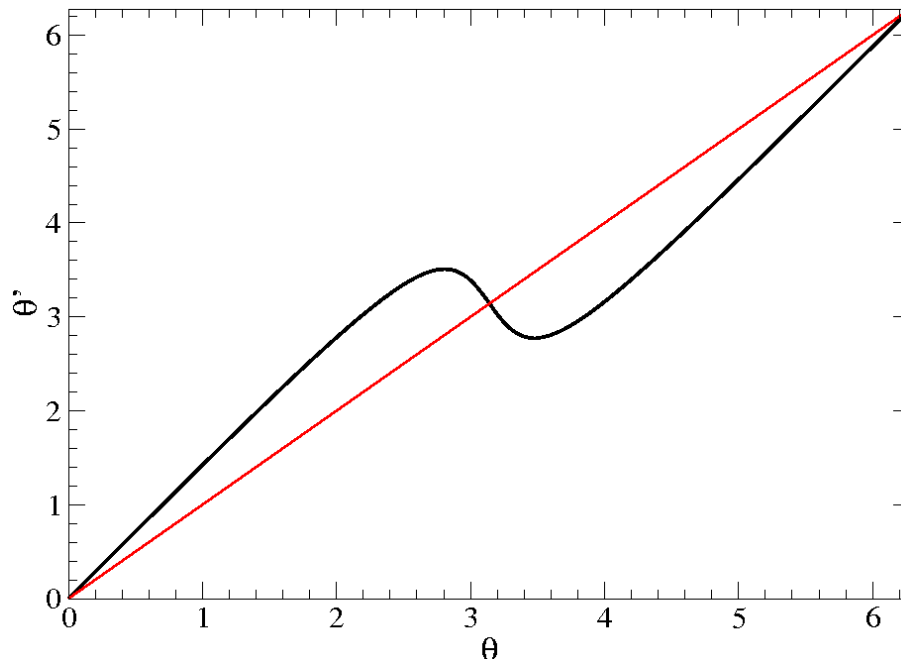


FIG. 2: The Gauss circle map is applied to the limaçon $r(\theta) = 2 + a \cos(\theta)$, with $a = 1.5$. This map is qualitatively the same as the more familiar Kolmogorov-Arnold circle map (7).

$$r(\theta, \phi) = 2 - a_1 \sin(\theta) + a_2 \cos(\phi) \quad (10)$$

It is useful to represent the Gauss sphere map $(\theta, \phi) \rightarrow (\theta', \phi')$ by representing the image by the point $x = (\phi' - \pi) \times \sin(\theta')$, $y = \theta'$. The area of the image is 4π , the area of the source.

The Gauss map for the sphere surface is invertible for $|a_1| + |a_2| < 1$ and noninvertible otherwise. For $|a_1| + |a_2| > 1$ the mapping exhibits singularities: either two cusps or four, depending on the values of the two parameters a_1 and a_2 . Fig. 3 shows the image of a patch of the sphere surface in the range $\frac{\pi}{2} - \frac{3}{4} \leq \theta \leq \frac{\pi}{2} + \frac{3}{4}$ and $\pi - \frac{3}{5} \leq \phi \leq \pi + \frac{3}{5}$ for $a_1 = 0.8$, $a_2 = 0.7$. The singularity has four cusps [14].

Sphere maps of various dimensions can be constructed that involve rigid rotations and nonlinear deformations of surfaces S^d defined by general limaçons

$$r(\theta_1, \theta_2, \dots, \theta_d) = 2 + \sum_{j=1}^d a_j \cos(\theta_j) \quad (11)$$

This family of maps is summarized in Table I.

V. SOME BIFURCATION SCANS

Under the map in Eq. (10) a point on the sphere will evolve, after transients have died out, to a fixed point, a mode locked orbit, a quasiperiodic trajectory, or a chaotic trajectory. Chaotic trajectories cannot occur unless the sphere map becomes noninvertible. In order to identify regions in the control parameter space $\omega, \mathbf{n}, \mathbf{a}$ or $(\omega_x, \omega_y, \omega_z), (a_1, a_2)$ where interesting behavior occurs, it is useful to carry out a number of scans. The first, shown in Fig. 4, identifies the number of distinct points in a trajectory as a function of rotation angle ω_z around the z axis as a function of increasing control parameters. The ratio of a_1 to a_2 is held fixed, and their values increase linearly from $(0, 0)$ at the bottom of the plot to $(0.8, 0.7)$ at the top. It is these parameter values for which the 4-cusp singularity is shown in Fig. 3. Mode-locked period one orbits are indicated by a dark blue color. Mode-locked period two orbits are shown

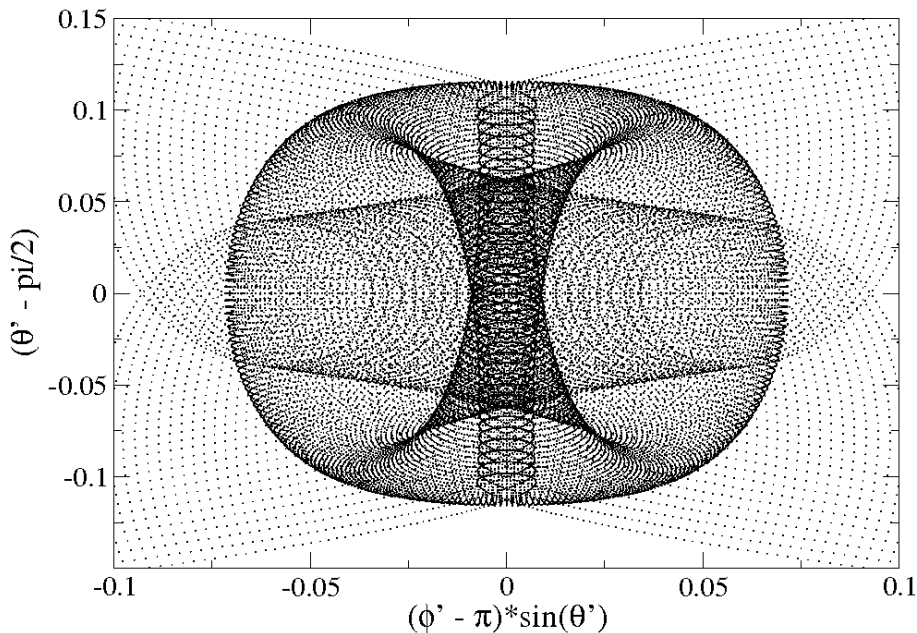


FIG. 3: For $1 < |a_1| + |a_2| < 2$ the spherical limaçon Eq. (10) has a nonsingular dimple. This means the Gauss sphere map is noninvertible ($1 < |a_1| + |a_2|$) and the surface defined by Eq.(10) is nonsingular with index 1 ($|a_1| + |a_2| < 2$). This plot shows how a rectangular 201×201 grid of points with $\frac{\pi}{2} - \frac{3}{4} \leq \theta \leq \frac{\pi}{2} + \frac{3}{4}$ and $\pi - \frac{3}{5} \leq \phi \leq \pi + \frac{3}{5}$ is mapped to a singularity on the sphere surface using the spherical limaçon (10) with $a_1 = 0.8, a_2 = 0.7$.

by a lighter blue color. The color coding for periodicity is shown in the color bar on the right. The region of period-one mode locking gradually increases with increasing nonlinearity parameters. Towards the top of this figure some chaotic behavior becomes apparent. For $|a_1| + |a_2| < 1$ only quasiperiodicity and mode locking are possible.

Fig. 5 is a scan involving rotation around the z axis. For this scan the values of the nonlinear parameters a_1 and a_2 are varied according to $a_1 = 1.6 * f, a_2 = 1.4 * (1 - f)$, where f varies from 0 at the bottom of the plot to $f = 1$ at the top. As f increases the singularity of the map proceeds from a double cusp in the a_2 direction near $f = 0$, to a quadruple cusp around $f = \frac{1}{2}$ (Fig. 3), and then back to a double cusp in the a_1 direction near $f = 1$.

A third scan is shown in Fig. 6. In this case the rotation is around the y axis and the rotation angle ω_y varies from 0 to 2π along the horizontal axis. The control parameters vary according to $a_1 = 0.48 * f$ and $a_2 = 0.42 * (1 - f)$, with f ranging from 0 to 1. For larger values of f mostly (but not entirely) mode-locked period-one behavior is seen. Comparable scans carried out with rotations around the x axis reveal almost entirely period-one mode-locking.

TABLE I: Sphere maps are generalizations of the circle map. These maps are compositions of two maps: a rigid rotation by a rotation group operation in $SO(n)$, and a nonlinear deformation of the sphere surface based on the Gauss map of a sphere to itself. The deformation is based on a generalized limaçon, given in Eq. (11). This table provides the number of parameters for each of the two maps and the nature of the generic singularity that can be encountered.

n	Group	Dim. Group	Sphere	Dim. Sphere	Singularity Type	Dim. "Sphere Map"
2	$SO(2)$	1	S^1	1	$A_2 + A_2$	2
3	$SO(3)$	3	S^2	2	$4A_3$	5
4	$SO(4)$	6	S^3	3	$2^3 A_4$	9
n	$SO(n)$	$\frac{1}{2}n(n-1)$	S^{n-1}	$n-1$	$2^{n-1} A_n$	$\frac{1}{2}(n+2)(n-1)$

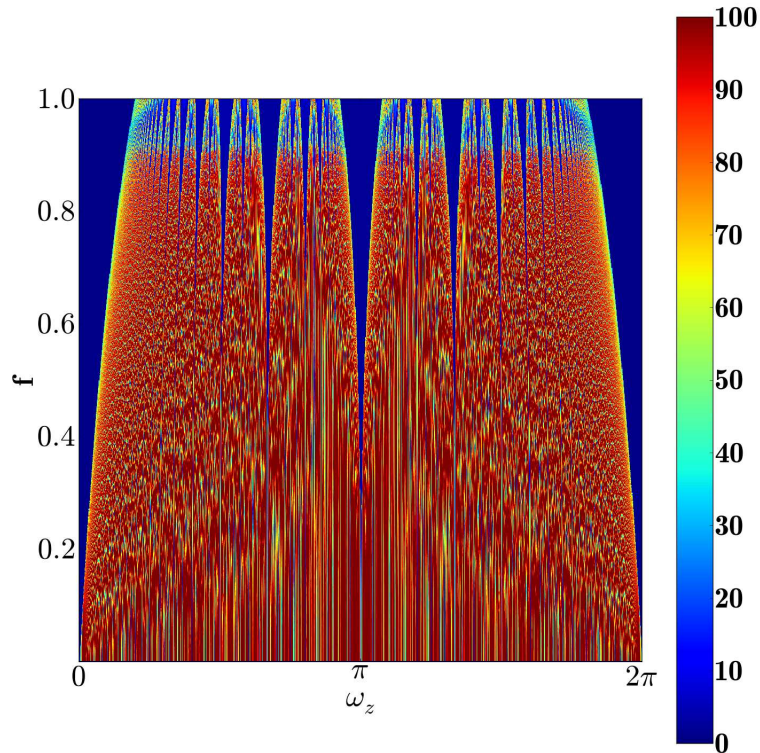


FIG. 4: (color online) Scan of the behavior exhibited by the sphere map. Horizontal axis: rotation angle ω_z around the z axis, $0 \leq \omega_z \leq 2\pi$. Vertical: strength of the nonlinearity, $a_1 = 0.8 * f$, $a_2 = 0.7 * f$ $0 \leq f \leq 1$. Color coding indicates the period of the trajectory. Cold colors (blues) indicate low period orbits. The hotter the color, the more distinct intersections the trajectory makes with the sphere surface. Such trajectories are either quasiperiodic or chaotic. Chaos cannot occur unless $|a_1| + |a_2| > 1$.

VI. BIFURCATION DIAGRAMS

Scans of the type shown in Figs. 4, 5, and 6 give a rough indication of where to look to find interesting behavior. Bifurcation diagrams provide a way to enlarge on that information. To illustrate, we have constructed a bifurcation diagram by taking a horizontal scan along Fig. 5 with $f = 0.25$. We plot $(\phi - \pi) \times \sin(\theta)$ for each of several hundred iterations (after transients have died out) as a function of rotation angle ω_z as the latter ranges from 0 to 2π (Fig. 7). This bifurcation diagram shows an admixture of low-period mode-locking, period-bubbling [15, 16, 17, 18], and quasiperiodic behavior.

Mode locking to a period- d orbit occurs at integer multiples of $\frac{2\pi}{d}$ radians. For example, period-one mode locking occurs around $\omega_z = 0$, period-two around $\omega_z = \frac{2\pi}{2} = \pi$ radians, period-three around $\omega_z = \frac{2\pi}{3}$ and $2 \times \frac{2\pi}{3}$, and so forth. The mode-locked regions are separated by regions with quasiperiodic orbits. The period-two and period-three mode locked regions show the beginning of a period doubling “cascade” that reverses very quickly. However, other higher mode-locked regions show period-doubling cascades that continue to and through the accumulation point before reversing in period-halving bifurcations. This is seen clearly in Fig. 8, which is a blowup of a small region of Fig. 7. In this figure we see very clearly the mode-locked period-four and period-five regions. In the period-four region there is a period-doubling cascade into chaos and a reverse cascade back to period-eight (c.f., Fig. 9). The reverse then reverses to period 16, 32, ..., back into chaos, and finally reverses back all the way down to period four before disappearing into a quasiperiodic sea. The behavior in the period-five window is even more complex.

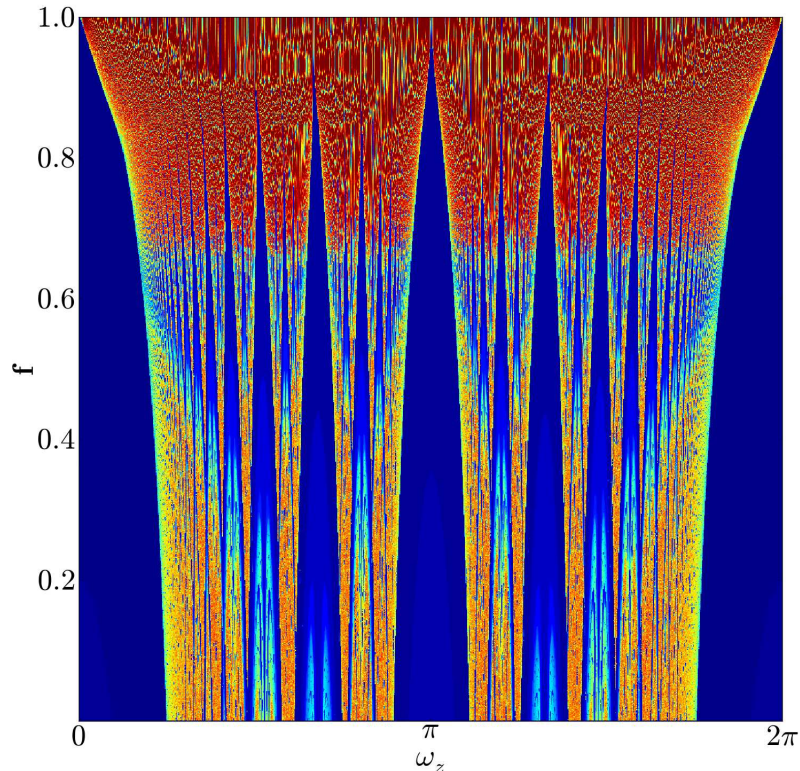


FIG. 5: (color online) Scan for which rigid rotations are about the z -axis with $0 \leq \omega_z \leq +2\pi$ (horizontal). The deformation parameters are $a_1 = 1.6 * f$, $a_2 = 1.4 * (1 - f)$ with f in the range $0 \leq f \leq 1$ (vertical). For $f < 0.7$ mode-locked regions are interspersed with regions supporting quasiperiodic orbits. For $f > 0.7$ period-doubling cascades lead to chaotic behavior.

VII. TRAJECTORIES

The nature of a trajectory can depend sensitively on control parameter values. In order to illustrate this point we have plotted the trajectories of the same initial condition (after transients have died out) for two slightly different control parameter values. The control parameter values are $\omega_z = 4.64, 4.80$ along the scan shown in Fig. 8. The results are shown in planar projection in Fig. 9. Both trajectories lie on the equator. One ($\omega_z = 4.64$) is the period-eight orbit between the pair of period-four bubbles in the period-four window that can be seen in Fig. 8. The eight points on the trajectory are indicated by the large circles. The other ($\omega_z = 4.80$) trajectory is a quasiperiodic orbit whose coordinates on the equator are represented by small points.

VIII. DISCUSSION AND CONCLUSION

Atomic coherent states are represented by points on the surface of a sphere S^2 . Under the action of a semiclassical hamiltonian $H_{s.c. atom}$ atomic coherent states evolve on the surface of the sphere. If the hamiltonian is time-independent the evolution is either a fixed point or a periodic orbit whose period is determined by the eigenvalues of the semiclassical hamiltonian (difference of adjacent eigenvalues). If the semiclassical hamiltonian is periodic the phase space expands from S^2 to $S^2 \times S^1$, the classical-like equations of motion for the point on the sphere representing the coherent state become more difficult to integrate, and motion can be quasiperiodic or chaotic.

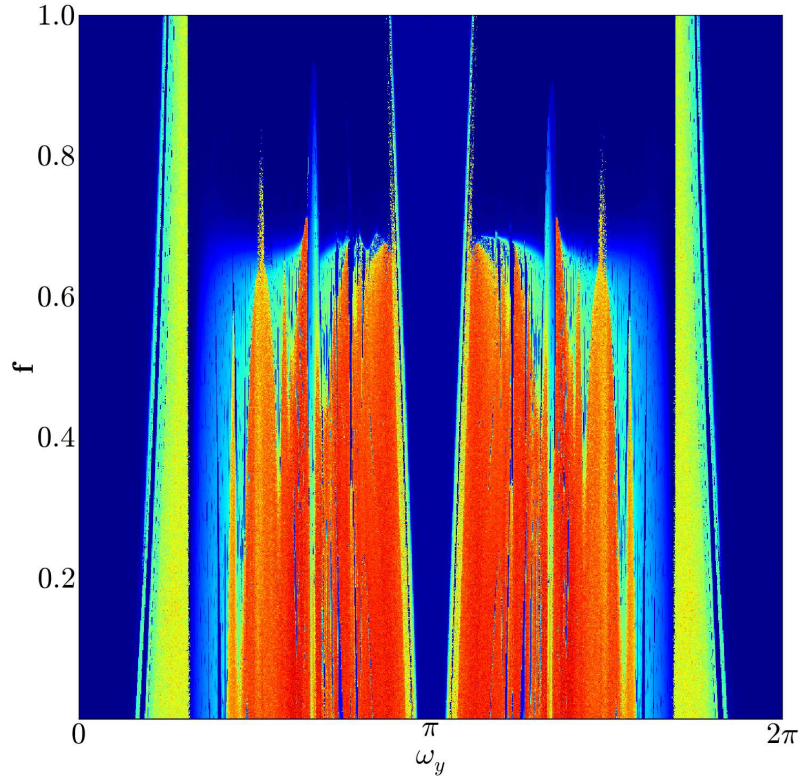


FIG. 6: (color online) Scan for which rigid rotations are about the y -axis with $0 \leq \omega_y \leq +2\pi$ (horizontal). The deformation parameters are $a_1 = 0.48 * f, a_2 = 0.42 * (1 - f)$ with f in the range $0 \leq f \leq 1$ (vertical). Mode-locked regions are interspersed with regions supporting quasiperiodic orbits. For this deformation parameter values the sphere map is invertible and chaotic behavior cannot occur.

In order to investigate the range of possible behaviors we studied the first return map for an arbitrary periodic drive. This is the map $S^2 \rightarrow S^2$, the sphere map. There are various ways to define a sphere map [8]. In this work we have chosen a natural generalization of the Arnold circle map. The generalization consists of the composition of two maps. One is “linear” in the sense that it is a rigid rotation of the sphere by the orthogonal group $SO(3)$. The second is a nonlinear deformation of the sphere surface. This deformation is constructed using the Gauss map of a surface to a sphere, where the surface is a two-parameter spherical limaçon. The two parameters are related to the two coordinate directions on the sphere surface. Generalization of such sphere maps to higher dimensions have been suggested. Our sphere map $S^2 \rightarrow S^2$ depends on three rotation parameters and two nonlinear parameters. We have verified that the member of the sphere map family $S^1 \rightarrow S^1$ on the circle is qualitatively the same as Arnold’s circle map. The comparison is shown in Figs. 1 and 2.

The sphere map is invertible until the parameter values become large enough. When the two parameters become large enough the map is noninvertible and chaotic behavior is in principle possible. The singularity type encountered in the transition from invertible to noninvertible is either a double cusp or a pair of double cusps, as shown in Fig. 3.

Three scans were taken to reveal roughly under what conditions the various types of behavior will exist. These are shown in Figs. 4, 5, and 6. Further investigation of the types of behavior suggested in these plots was carried out with bifurcation plots, as seen in Fig. 7. This figure shows harmonic mode-locked regions with basic orbits of period n sandwiched between regions in which quasiperiodic orbits are present. Further, the mode-locked orbits of period n undergo period doubling cascades that eventually reverse back to period n . Some period “bubbling” bifurcations are clearly evident in Fig. 8. The distinction between periodic orbits and quasiperiodic orbits is clearly made in Fig. 9.

We have just begun to explore the rich variety of behaviors that the sphere map $S^2 \rightarrow S^2$ can exhibit.

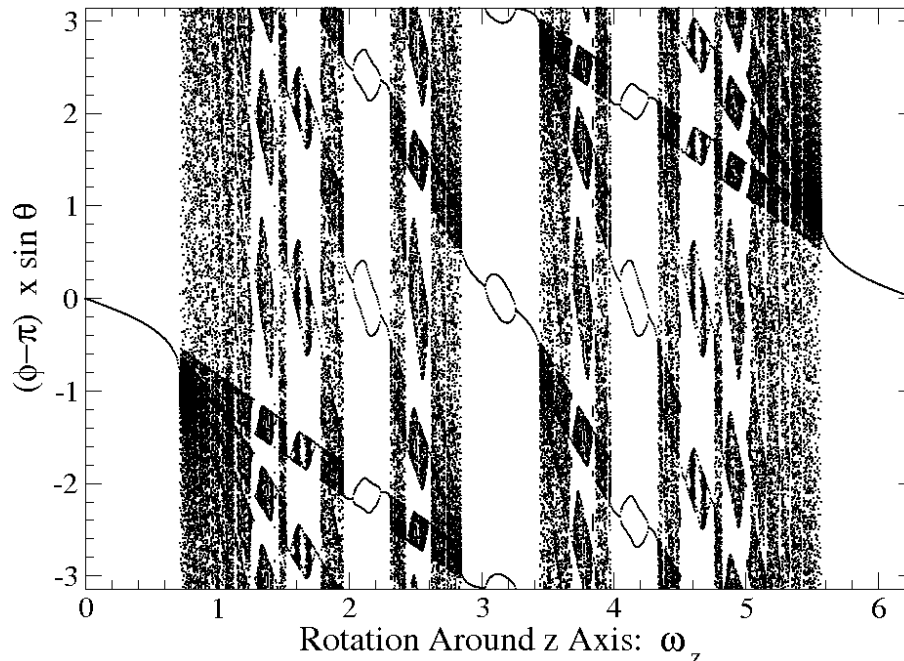


FIG. 7: A bifurcation diagram is obtained by plotting the value of $(\phi - \pi) \times \sin(\theta)$ against the angle of rigid rotation around the z -axis, ω_z , for $a_1 = 1.6 \times f$, $a_2 = 1.4 \times (1 - f)$ and $f = 0.25$. This diagram shows regions of direct and inverse period-doubling, quasiperiodic orbits, and chaos. Period-two (and four) orbits exist around $\frac{2\pi}{2}$, period three orbits (and multiples) exist around $\frac{2\pi}{3}$ and $2 \times \frac{2\pi}{2}$, etc. Although ϕ varies from iteration to iteration, $\theta = \pi/2$ throughout this range of rotation angle values.

This work was supported in part by NSF Grant PHY 0754081.

REFERENCES

- [1] F. T. Arecchi, E. Courtens, R. Gilmore, and H. Thomas, Atomic coherent states in quantum optics, *Phys. Rev.* **A6**, 2211-2237 (1972).
- [2] E. Schrödinger, The continuous transition from micro- to macro-mechanics, *Naturwissen.* **14**, 664-666 (1926).
- [3] R. J. Glauber, The quantum theory of optical coherence, *Phys. Rev.* **130**, 2529-2539 (1963).
- [4] R. J. Glauber, Coherent and incoherent states of the electromagnetic field, *Phys. Rev.* **131**, 2766-2788 (1963).
- [5] R. J. Glauber, *Quantum Theory of Optical Coherence. Selected Papers and Lectures*, Weinheim: Wiley-VCH, 2007.
- [6] E. A. Jackson, *Perspectives on Nonlinear Dynamics*, Cambridge: University Press, 1989.
- [7] R. Gilmore and M. Lefranc, *The Topology of Chaos*, NY: Wiley, 2002.
- [8] K. Gilmore and R. Gilmore, Introduction of the sphere map with application to spin-torque nano-oscillators, *World Scientific Review* (in press).
- [9] V. I. Arnold, Small denominators and problems of stability of motion in classical and celestial mechanics, *Russian Math. Surveys* **18**(6), 85-191 (1963).
- [10] V. I. Arnold, Small denominators. I. On the mappings of the circumference onto itself, *Trans. Am. Math. Soc.* 2nd Ser. **46**, 213 (1965).
- [11] E. P. Wigner, *Group Theory*, NY: Academic Press, 1959.
- [12] R. Gilmore, *Lie Groups, Lie Algebras and Some of Their Applications*, NY: Wiley, 1974.
- [13] D. J. Struik, *Differential Geometry*, Reading, MA: Addison-Wesley, 1950.
- [14] R. Gilmore, *Catastrophe Theory for Scientists and Engineers*, NY: Wiley, 1981.
- [15] U. Parlitz and W. Lauterborn, Resonances and torsion numbers of driven dissipative nonlinear oscillators, *Z. Naturforsch.* **41a**, 605-614 (1986).
- [16] U. Parlitz, V. Englisch, C. Scheffczyk, and W. Lauterborn, Bifurcation structure of bubble oscillators, *Acoust. Soc. Am.* **88**, 1061-1077 (1990).

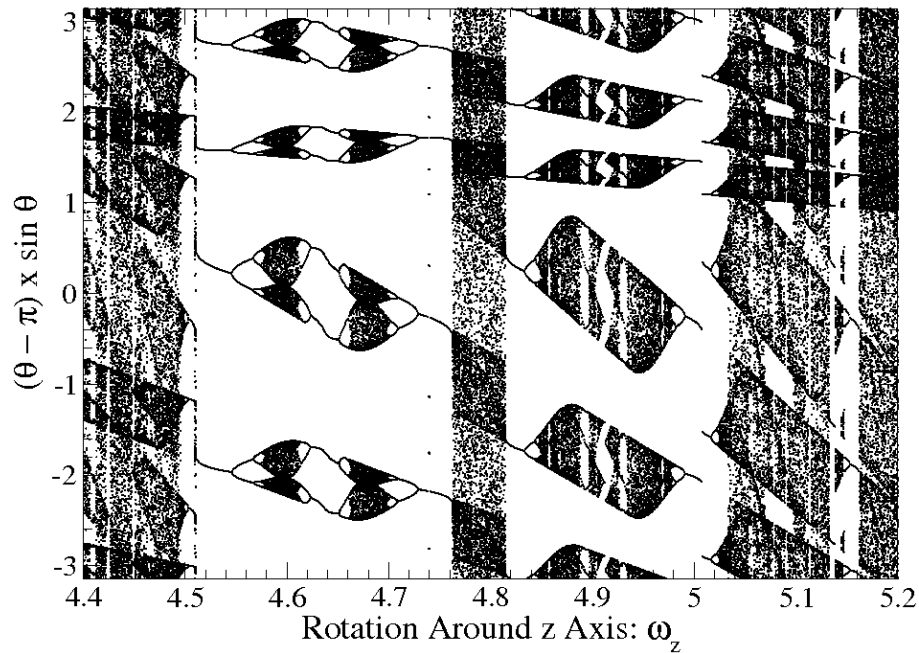


FIG. 8: Blowup of Fig. 7 for the same parameter values. This clearly shows that regions of quasiperiodicity are separated by regions of modelocking based on period 3 (to the left of 4.4), 4, 5, 6, Each of the mode-locked regions seen here proceeds through a period-doubling cascade to chaos, and then unwinds this process in a period-halving cascade back to the basic mode-locked period, before disappearing into quasiperiodic behavior.

- [17] R. Gilmore and J. W. L. McCallum, Superstructure in the bifurcation diagram of the Duffng oscillator, *Phys. Rev.* **E51**, 935-956 (1995).
 [18] R. Gilmore, Topological analysis of chaotic dynamical systems, *Revs. Mod. Phys.* **70**, 1455-1530 (1998).

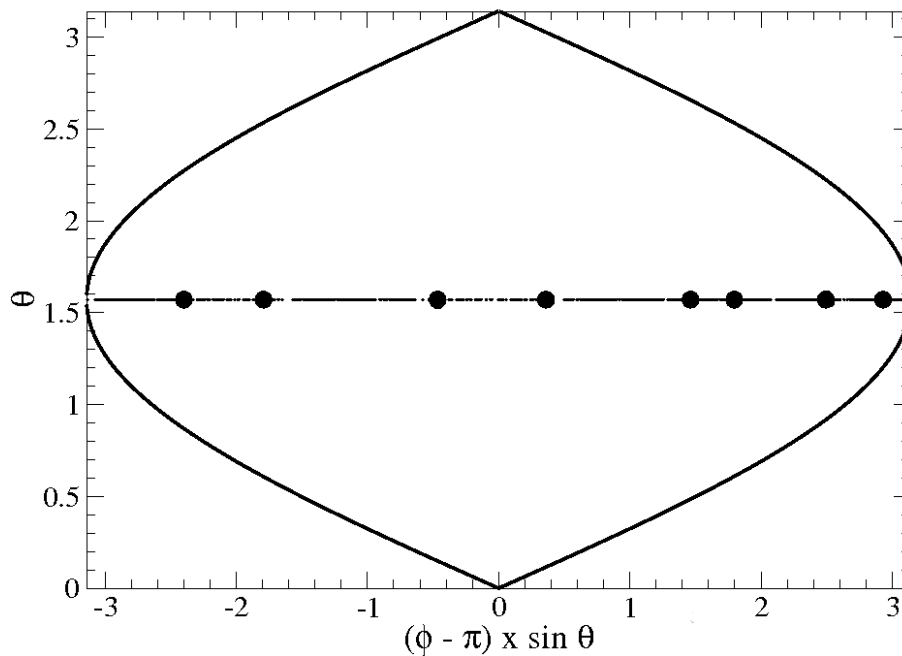


FIG. 9: Nearby control parameter values produce trajectories with distinctly different properties. A mode-locked period-eight trajectory is generated with $\omega_z = 4.64$ in Fig. 8, and the quasiperiodic trajectory corresponds to $\omega_z = 4.80$. The coordinates (θ, ϕ) defining a point on the surface S^2 are mapped into the points $((\phi - \pi) \times \sin(\theta), \theta)$. The boundary of this region is shown. The area enclosed is 4π . For both trajectories the value of the θ coordinate is $\frac{\pi}{2}$ for all points.